# A Direct $Ku$-Band Linear Subharmonically Pumped BPSK and I/Q Vector Modulator in Multilayer Thin-Film MCM-D

Geert J. Carchon, *Student Member, IEEE*, Dominique M. M.-P. Schreurs, *Member, IEEE*, Walter De Raedt, Paul Van Loock, and Bart K. J. C. Nauwelaers, *Senior Member, IEEE*

***Abstract*—A direct $Ku$-band linear subharmonically pumped binary phase-shift keying (BPSK) and in-phase/quadrature (I/Q) vector modulator have been developed using multilayer thin-film multichip module (MCM-D) technology. All passives are integrated in the low cost MCM-D substrate. To the authors knowledge, this is the first modulator based on thin-film integrated passive components. The subharmonic mixing is performed using a beam-lead antiparallel diode pair mounted onto the MCM using thermocompression. A custom diode model has been developed and verified using nonlinear network analyzer measurements: an excellent agreement between the measured and simulated powers and phases for more than nine harmonics is demonstrated. Additionally, it is shown that an optimal reactive termination for the third harmonic of the local oscillator (LO) exists such that a very flat BPSK mixer conversion is obtained. This is validated by measurements that indicate a ±0.25-dB variation on the conversion loss for an LO frequency varying from 6.8 to 7.6 GHz. The I/Q vector modulator consists of a Wilkinson power divider, a coplanar-waveguide Lange coupler, and two BPSK modulators. It has a measured image rejection better than −27 dB over the RF range of 13.4–15.2-GHz band (corresponding to a vector phase and amplitude error lower than 2° and 1%). The image rejection is even better than −32 dB over the very small aperture terminal band (RF: 14–14.5 GHz).**

***Index Terms*—BPSK modulator, integrated passives, MCM-D, QPSK modulator.**

## I. Introduction

ZERO-IF or direct digital modulation at microwave frequencies has gained considerable interest for some years now due to the simplicity and compactness of the transmitter [1]–[4]. Compared to modulation schemes using one or more IF frequencies, it offers several advantages such as a reduction in power consumption, board space, hardware (upconvertors and filters), and the achievement of high-modulation bandwidths. Typical applications are found in satellite transmission with on-board signal processing and microwave digital radio links.

Subharmonic mixing is attractive due to the inherent local oscillator (LO)/RF isolation. For mixing at an even harmonic of the LO, subharmonic mixers (SHMs) typically use a nonlinear device with an antisymmetric current–voltage characteristic such as an antiparallel Schottky barrier diode pair [5].

Recent realizations primarily use GaAs monolithic-microwave integrated-circuit (MMIC) technology [1]–[4], which results in an expensive solution. Moreover, only a small part of the chip area is consumed by the active devices such as buffer transistors and diodes. Another more cost-effective solution is to use multilayer thin-film multichip module (MCM-D) technology. It offers a very high reproducibility of small dimensions and is, therefore, a promising technology for the low-cost integration of RF and microwave circuits [6], [7]. Moreover, the availability of low-loss transmission lines and high-$Q$ inductors allows the realization of filters and matching circuits with losses that are significantly lower as compared to MMIC technologies [8].

Traditionally, MCM-D has been developed as a high-performance packaging and interconnect technology. With the availability of high-performance integrated passives, a high degree of integration can be obtained, hereby reducing size and weight, but also cost and power consumption, as compared to previous hybrid solutions. Up to now, integrated passives have primarily been focused toward passive applications at lower microwave frequencies; however, they can also be used for the realization of more complex microwave circuits.

In this paper, a direct linear subharmonically pumped $Ku$-band binary phase-shift keying (BPSK) and in-phase/quadrature (I/Q) vector modulator in multilayer thin-film MCM-D are presented. All passives are integrated using the low-cost high-performance MCM-D technology. No tuning on the circuits has been performed. To the authors knowledge, this is the first modulator based on thin-film integrated passive components. Additionally, it is shown that an optimal reactive termination for the third harmonic of the LO exists such that a very flat BPSK mixer conversion is obtained. This is validated by measurements that indicate a ±0.25-dB variation on the conversion loss for an LO frequency varying from 6.8 to 7.6 GHz.

In Section II, we will briefly introduce the MCM-D technology and available passive components. In Section III, the developed nonlinear diode model will be validated using nonlinear

Manuscript received November 3, 2000. This work was supported by the Flemish Institute for the Advancement of Scientific-Technological Research in Industry under a scholarship, by the European Space Agency under Contract 13627/99/NL/FM(SC), and by Agilent Technologies under a Non-Linear Network Measurement System donation.

G. J. Carchon and W. De Raedt are with Division MCP-HDIP, Interuniversity Microelectronics Centre, B-3001 Leuven, Belgium (e-mail: geert.carchon@imec.be).

D. M. M.-P. Schreurs and B. K. J. C. Nauwelaers are with the Division of Electronics, Systems, Automation, and Technology-Division TELEMIC, Katholieke Universiteit Leuven, B-3001 Leuven, Belgium.

P. Van Loock is with Alcatel Bell Space, B-2660 Hoboken, Belgium.

Publisher Item Identifier S 0018-9480(01)06146-4.

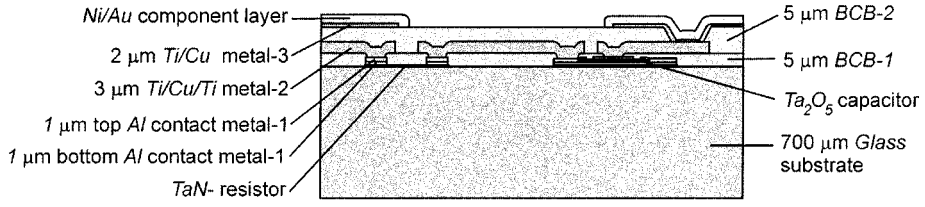


Fig. 1. Layer buildup of IMEC's MCM-D technology.

network analyzer measurements. The design method and measured results of the BPSK modulator will be given in Section IV, while in Section V, the design and measurements of the QPSK modulator will be discussed.

## II. Integrated Passives MCM-D Technology

The used MCM-D technology (the layer buildup is shown in Fig. 1) consists of alternating thin layers of photosensitive benzo-cyclobutene (BCB) dielectric (Cyclotene from Dow Chemical, Midland, MI) and low-loss copper metallizations deposited on a borosilicate glass carrier substrate ($\varepsilon_r = 6.2$, $\tan\delta \approx 9.10^{-4}$). The BCB dielectric has very low dielectric losses ($\tan\delta \approx 5.10^{-4}$), a low dielectric constant ($\varepsilon_r = 2.65$), and a low moisture absorption. The material is spin coated in 5-$\mu$m-thin films and then developed and cured. The curing temperature profile of BCB does not exceed 250 °C, which is significantly lower than for most other dielectric materials (such as, e.g., polyimide). The 3-$\mu$m-thick copper metal layer is sandwiched between two 30-nm-thick titanium layers, rendering good adhesion. This metal layer is realized by electroplating on a thin titanium–copper seed layer. Via holes through the BCB dielectric allow the connection of the different metal layers. The vias have a typical diameter of 30 $\mu$m, although smaller values are possible.

A coplanar waveguide (CPW) design methodology is used, as this has several advantages over the more traditional microstrip approach. No through-substrate vias are required and backside wafer processing is omitted. The standard CPW line is located on the middle low-loss Cu metal layer. Typical losses are $-0.07$ dB/mm at 20 GHz for the standard 50-$\Omega$ line (77-$\mu$m width, 20-$\mu$m slot).

The TaN resistors (typical value of 25 $\Omega/\square$) and $Ta_2O_5$ capacitors are realized immediately on the carrier substrate, as they require a high-temperature annealing step. This is not compatible with the relatively low-temperature steps for the subsequent BCB layers.

Two types of metal–insulator–metal (MIM) capacitors can be used. For the larger capacitance values, a layer of anodized tantalum (720 pF/mm$^2$) is realized on the glass carrier substrate. These $Ta_2O_5$ capacitors are contacted with Al-based contact metal. For the small capacitors (4.7 pF or 9.4 pF/mm$^2$, depending on the type), BCB is used as the insulating dielectric.

High-$Q$ spiral inductors are integrated in the Cu metal layer in a coplanar style. Layouts separately optimized for low cost (corresponding to narrow strips and slots and a small gap to the ground plane) or high performance (wider strips and slots and a larger distance to the ground plane) are available. The quality factors of the inductors may go above 100 at 10 GHz (inductances $<$ 1.7 nH). Naturally, for larger inductances, a lower quality factor will be obtained due to the increased losses and capacitive coupling between the turns. However, an inductor of 18 nH still has a maximum $Q$ of 38 at 2 GHz, while a 40-nH inductor still has a $Q$ of 29 at 1 GHz. The $Q$ values are, therefore, significantly higher than those reported on MMICs. This will allow the realization of low-loss filters, hereby resulting in an improved conversion loss.

All passive components and discontinuities have been modeled and integrated in a design library [9]–[12], which allows the realization of a variety of low-loss passive circuits [8].

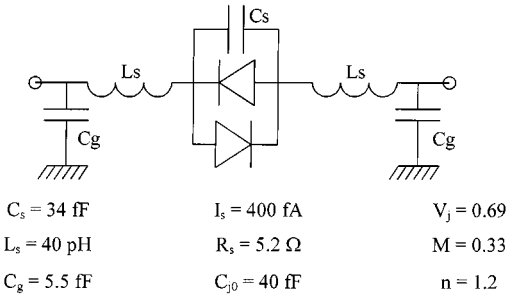


Fig. 2. Model used for the APDP, excluding the mounting pads.

## III. Diode Model

Besides accurate scalable models for the integrated passives, a good diode model is required. We have used the GaAs HSCH-9251 beam-lead antiparallel diode pair (APDP) to perform the subharmonic mixing. It has been mounted on the MCM using thermocompression.

The custom model for the beam-lead APDP, excluding the mounting pads, is shown in Fig. 2. The simulator's (Agilent ADS, Santa Rosa, CA) built-in diode model was used to represent the intrinsic diodes, as this allows to easily evaluate the sensitivity of the overall circuit performance to the intrinsic diode parameters. The mounting parasitics (feeding lines) were modeled using the equivalent models of the custom design library. The intrinsic and extrinsic parameters have been constructed based on dc- and $S$-parameter measurements of the corresponding single diode (HSCH-9101) (using the procedure outlined in [13] and [14]).

The diode model has been verified using two-port nonlinear network analyzer measurements [15]. An excellent agreement can be observed between the measured and simulated powers and phases for more than nine harmonics in Fig. 3. The measurements have been performed on a single diode in series con-

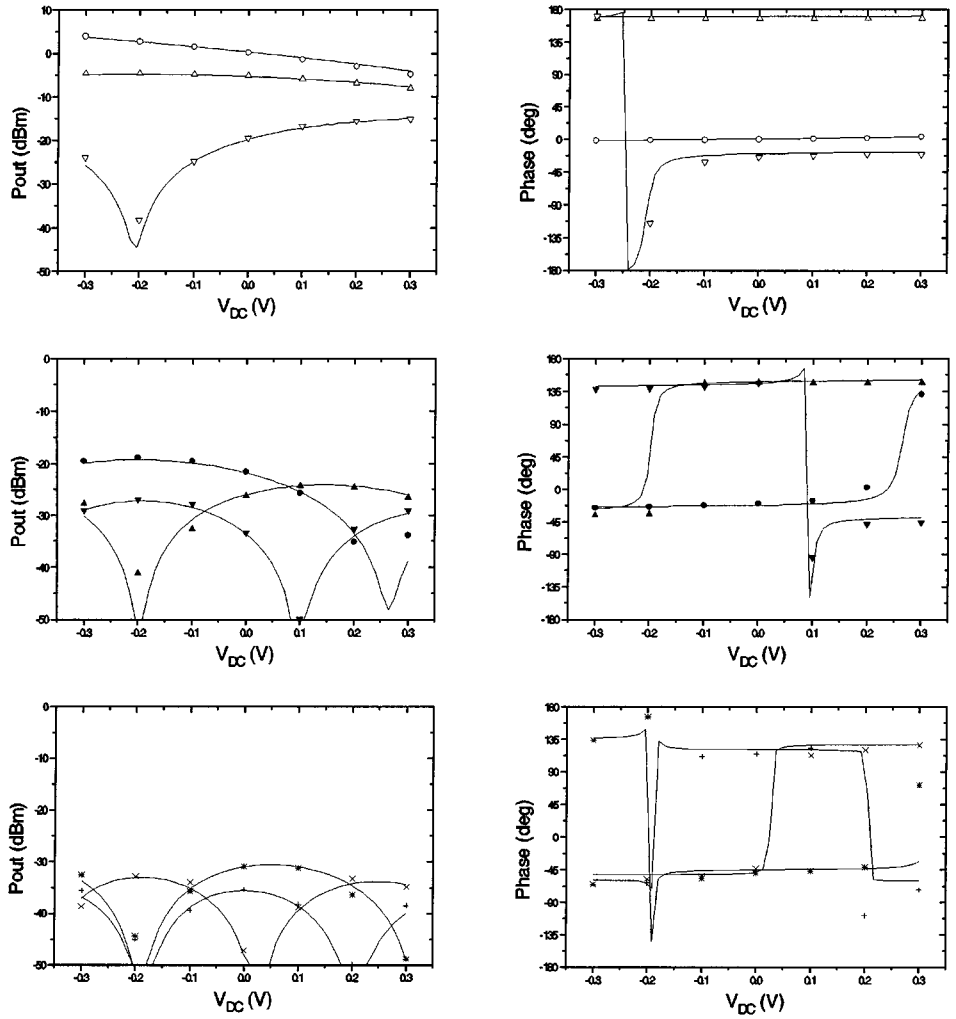


Fig. 3. Simulated (−) versus measured (marks) power (left-hand side) and phase (right-hand side) at the fundamental (9.5 dBm at 1 GHz) and harmonics: (○) fundamental, (△) second, (▽) third, (●) fourth, (▲) fifth, (▼) sixth, (∗) seventh, (×) eighth, and (+) ninth harmonic.

figuration, excited with 9.5 dBm at 1 GHz (cathode). The fundamental and harmonics were measured at the output port (anode) for different dc-biasing conditions applied at the anode.

## IV. BPSK Modulator

The I/Q linear vector modulator has been developed for very small aperture terminal (VSAT) applications (RF: 14–14.5 GHz, subharmonic LO: 7–7.25 GHz). The design band of the modulators was taken in the 13.6–14.9-GHz range.

### *A. Architecture and Harmonic Termination*

The mixer uses the APDP mounted in a shunt-to-ground configuration [16] in combination with a triplexer structure.

One of the key requirements of the BPSK modulator was to obtain a very flat conversion loss as a function of LO frequency. A good and constant LO and RF return loss are also important when the BPSK mixer is used in the realization of the I/Q modulator. This will be obtained by an optimal harmonic loading of the third harmonic of the LO.

The conversion loss and input impedances heavily depend on the phase of the reactive termination of the third harmonic of the LO. This can be concluded from Fig. 4, where the simulated LO-, RF- and IF-input impedance and the IF-to-RF conversion loss are given as a function of the phase of the third harmonic reactive termination of the LO. The simulation was performed at 7 GHz and ideal bandpass filters were assumed in the triplexer structure of the SHM. All other harmonics (fourth and higher) of the LO were terminated on a short. The latter termination was, however, not so important.

We may conclude that if the third harmonic is terminated with the proper phase, a flat LO-, RF-, and IF-input impedance may be obtained over a reasonable bandwidth. This is essential to obtain a good and constant matching (one should keep in mind that the conversion and embedding impedances should be constant over a range of phases as, e.g., a $\lambda/4$ line at 7 GHz, already results in a phase variation of about 25° over the 20.4–22.35-GHz band). Naturally, the conversion loss is related to the embedding impedances. A flat conversion loss can be obtained in the same region.

### *B. Design*

The architectural implementation of the triplexer is shown in Fig. 5. The requirements on the IF and RF filter are only moderate due to the presence of the LO block filter. The IF filter is

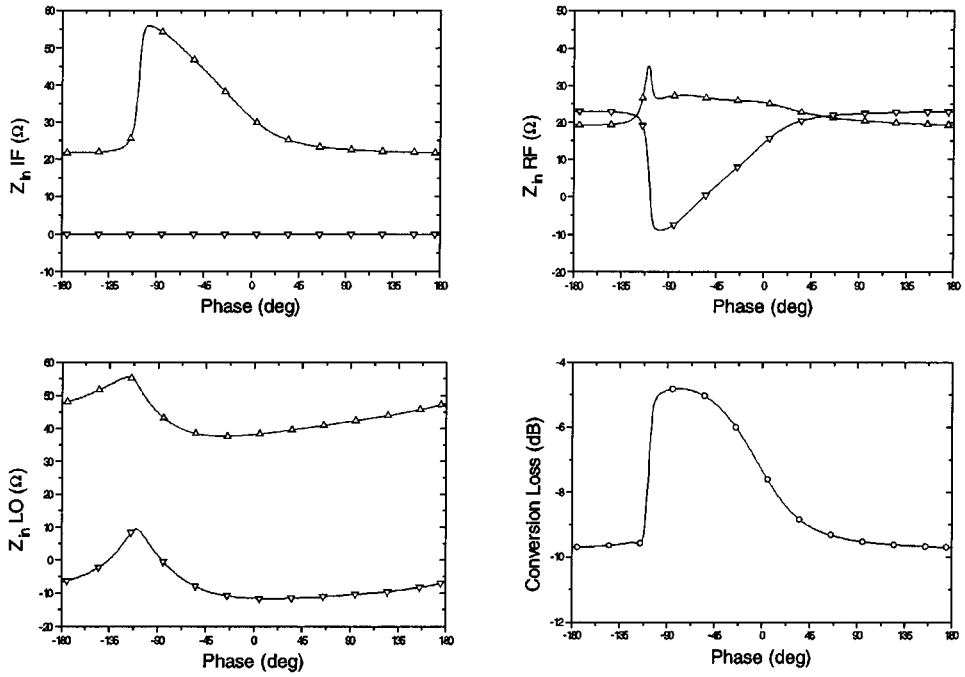


Fig. 4. LO, IF, and RF input impedance ($\triangle$: real part, $\nabla$: imaginary part) and IF-to-RF conversion as a function of the phase of the reactive termination of the third harmonic of the LO (10-dBm input power at 7 GHz, $\mathrm{IF} = 10$ MHz, $\mathrm{RF} = 14.01$ GHz).

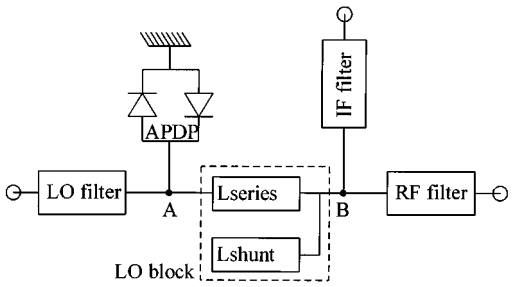


Fig. 5. Architectural implementation of the BPSK modulator.

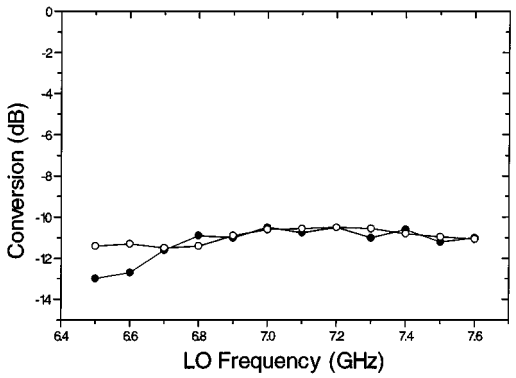


Fig. 6. Measured (•) versus simulated (∘) conversion loss as a function of LO frequency.

a fourth-order low-pass filter, providing an open at the RF frequency. The RF filter is a third-order high-pass filter, providing an open at the IF frequency.

$\mathrm{L_{shunt}}$ is a $\lambda/4$ transmission line at 7.1 GHz, which provides a short at point B for the LO and the third harmonic. Hence, the harmonic termination is well defined at point B and is not influenced by circuits cascaded with the BPSK modulator. $\mathrm{L_{series}}$ can be tuned in combination with the LO filter to provide an optimal third harmonic termination at point A, while at the same time, matching the diode at the LO frequency. Other requirements for the LO filter are to provide an open at the RF and IF frequencies.

The LO filter has been realized as a fourth-order low-pass filter cascaded by a third-order high-pass filter, as this allowed to simultaneously fulfill all constraints. Due to the low-pass filter structure, the harmonic termination is well defined at point A and is not influenced by the impedances presented by the circuits cascaded with the modulator. The incorporated low-pass filter further offers embedded filtering for the second harmonic of the output spectrum of the voltage-controlled oscillator (VCO).

The APDP is pumped with 10-dBm LO power. The circuit measures $3.3 \times 14.1$ mm$^2$. DC biasing is not required.

### *C. Measurements*

The measured versus simulated conversion loss as a function of LO frequency is given in Fig. 6. An excellent agreement can be observed, which indicates the high quality of the used models. A very flat behavior ($-10.8 \pm 0.3$) dB is obtained due to the correct harmonic loading of the third harmonic of the LO.

The measured phase balance (using the nonlinear network measurement system) of the BPSK modulator is shown in Fig. 7. Over the 13.0–15.2-GHz band, the phase balance is nearly perfect and equals ($180^\circ \pm 0.5^\circ$). This is due to the good current–voltage characteristics of the APDP.

The LO return loss is better than $-14$ dB over the 6.8–7.6-GHz band, while the RF return loss is better than $-12.5$ dB over the 13.6–15.4-GHz band.

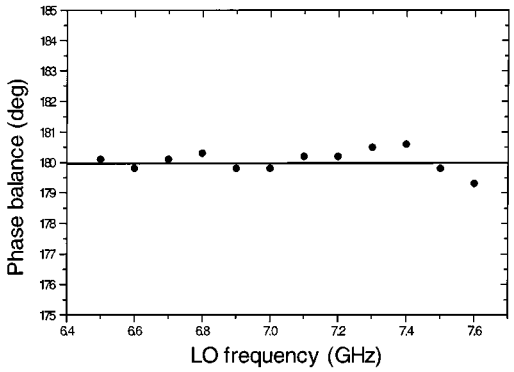


Fig. 7. Measured phase balance of the BPSK modulator.

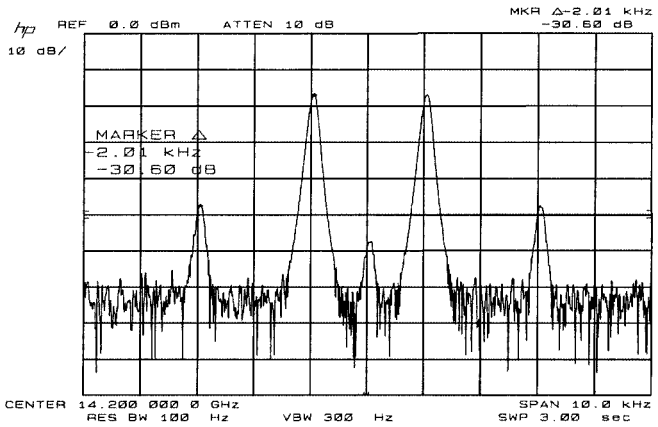


Fig. 8. Measured output spectrum of the BPSK modulator: a linear output power of −10 dBm per sidelobe is possible with the harmonics of the modulating frequency below −31 dB.

The modulator has a maximum linear output power of −10 dBm (in each sideband) with the harmonics of the modulating frequency remaining below −31 dB. The suppression of the LO fundamental is −30 dB at the output (−20 dBm), while the second harmonic of the LO is more than −40 dB below the BPSK signal. The corresponding output spectrum is shown in Fig. 8.

When the modulator is used in a system, the second harmonic of the VCO should be suppressed. This is also performed by the LO filter having a measured −22-dB suppression of the second harmonic of the LO.

## V. Linear I/Q Vector Modulator

The chip was designed to perform QPSK modulation, however, as it is a linear vector modulator, any digital modulation scheme can be implemented.

The architecture of the QPSK modulator is shown in Fig. 9: the modulator is obtained by combining two BPSK subharmonic modulators, a Wilkinson power divider, and a CPW Lange coupler. The Wilkinson power divider is used to split the LO power and isolate the BPSK modulators. The quadrature coupler is used for the summation of the output of the BPSK modulators, hereby providing 90° phase shift. It should also isolate both BPSK modulators. A Lange coupler has been selected due to its good isolation, amplitude, and phase balance.

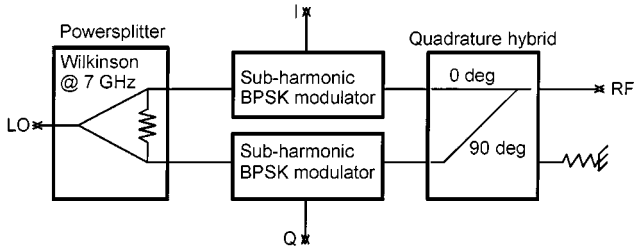


Fig. 9. Architecture of the realized QPSK modulator.

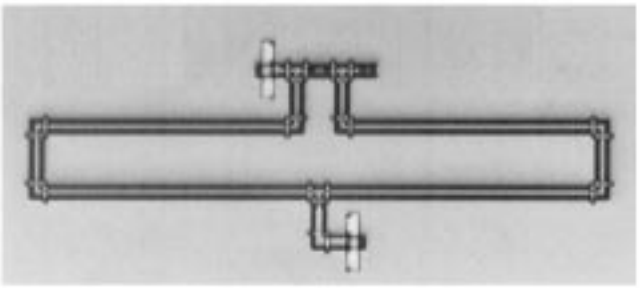

Fig. 10. Implemented distributed Wilkinson power divider.

Tunable on-chip phase shifters and buffer amplifiers (to increase the isolation between the APDPs) have not been added. This tightens the requirements on the Lange couplers return loss and isolation, but also on the BPSK RF return loss. However, the resulting I/Q vector modulator does not require any dc biasing or tuning and can be realized with a minimum number of external components.

### A. Passive Circuits

*1) Wilkinson Power Divider:* The Wilkinson power divider has been developed using the custom design library [9]. A fully distributed design (Fig. 10) was selected, as it allows an easy layout of the modulator. Smaller realizations with comparable performance are, however, also possible [17].

Over the 6.5–7.6-GHz band, the Wilkinson power divider has a measured return loss better than −22 dB, an isolation better than −25 dB with only −3.33-dB insertion loss (−3 dB is due to the power split). An excellent correspondence between the measured and simulated $S$-parameters has been obtained, as can be seen from Figs. 11 and 12. This indicates the high accuracy that can be obtained using the MCM-D passive components and models.

*2) Quadrature Lange Coupler:* The design method for the CPW Lange couplers has been outlined in [18]. A picture is shown in Fig. 13, and the measured results are shown in Figs. 14 and 15. In the 10.5–14.5-GHz band, the Lange coupler has a measured return loss and isolation better than −20 dB, an amplitude balance below 0.2 dB and a phase balance of $(90^\circ \pm 1^\circ)$. A low insertion loss of −3.35 dB has been obtained (−3 dB is due to the power split). This can be attributed to the Cu metallizations and the low-loss dielectrics.

### B. Design

Due to the finite isolation of the Lange coupler and the finite RF return loss of the BPSK modulators, small phase imperfec-

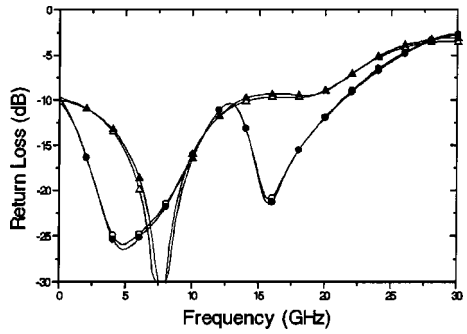


(a)

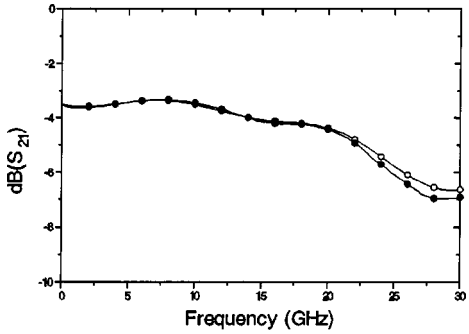


(b)

Fig. 11. Measured (full) versus simulated (open): (a) return loss and (b) thru for the Wilkinson power divider.

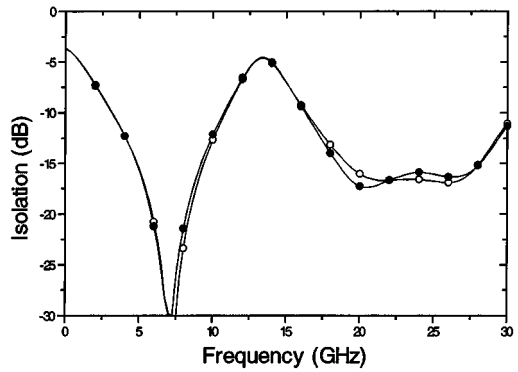


Fig. 12. Measured (•) versus simulated (∘) isolation for the Wilkinson power divider.

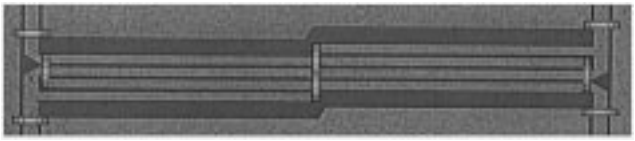

Fig. 13. CPW Lange coupler.

tions occur in the resulting QPSK constellation. This has been compensated by cascading a short high- and low-impedance line with the top and bottom BPSK modulator. The terminating impedance of the Lange coupler's fourth port was also optimized to obtain a perfect amplitude and phase balance. The developed QPSK modulator is shown in Fig. 16. The circuit measures $7.6 \times 16.9$ mm$^2$.

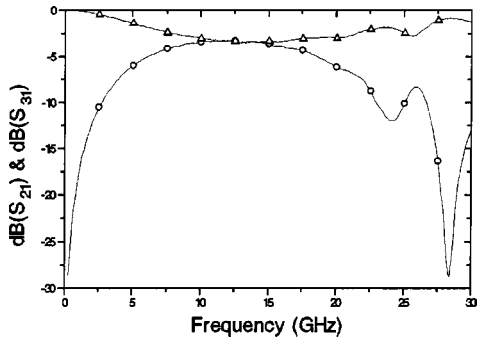


(a)

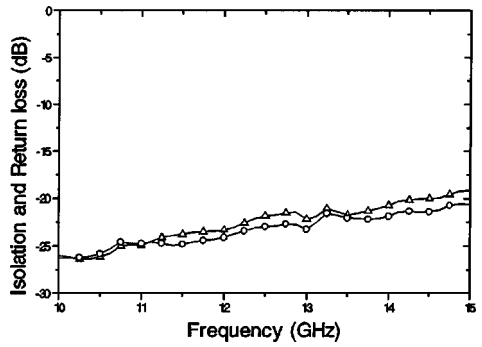


(b)

Fig. 14. Measured thru (△) and coupled (∘): (a) port and (b) return loss (△) and isolation (∘) for the four-finger CPW Lange coupler.

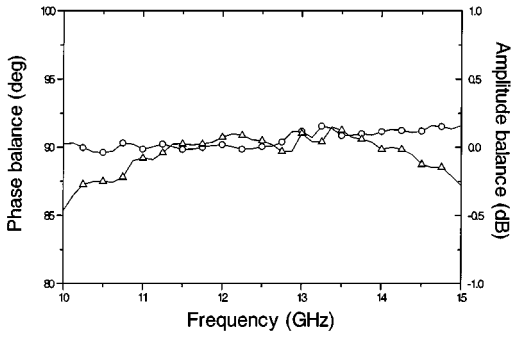


Fig. 15. Measured amplitude (△) and phase (∘) balance for the CPW Lange coupler.

### *C. Measurements*

Both spectral as constellation measurements have been performed.

As each BPSK modulator is pumped with 10 dBm, the total required LO power for the I/Q vector modulator is 13 dBm. At the output, the fundamental is more than $-30$ dB lower over the entire design band.

The measurement of the single-sideband (SSB) spectrum is very useful for the characterization of the modulator, as it directly reveals the rejection of all undesired frequency components and circuit imperfections: carrier, image (due to quadrature imperfections), and in-band spurious responses (due to nonlinearity of the modulation) [3]. For this purpose, an orthogonal I and Q signal are applied to the modulator.

The measured SSB output spectrum (LO $=$ 7.1 GHz) is shown in Fig. 17: a maximum linear output power of $-10$ dBm is possible (harmonics of the modulating frequency below

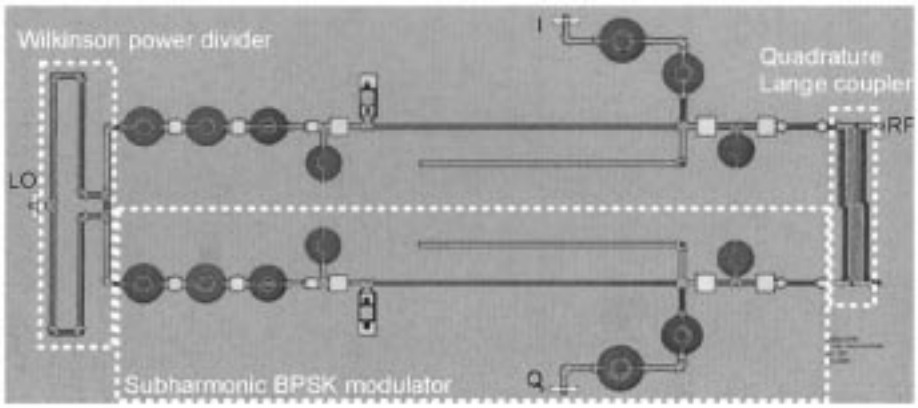


Fig. 16. Developed I/Q vector modulator.

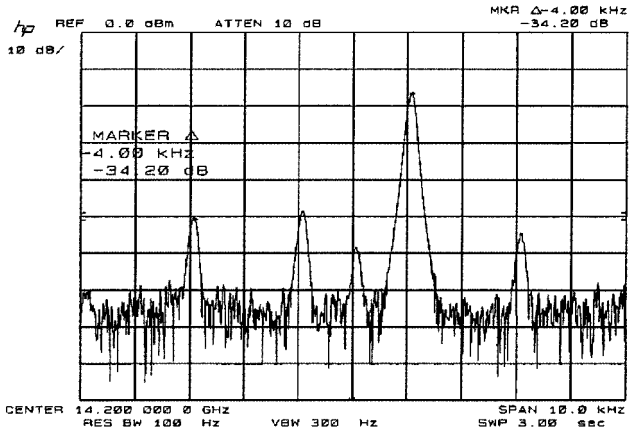


Fig. 17. Measured SSB output spectrum: a linear output power of −10 dBm is possible with the harmonics of the modulating frequency below −34 dB.

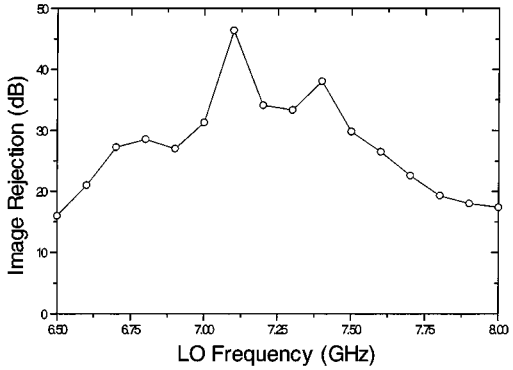


Fig. 18. Measured image rejection (- ∘ -) as a function of LO frequency.

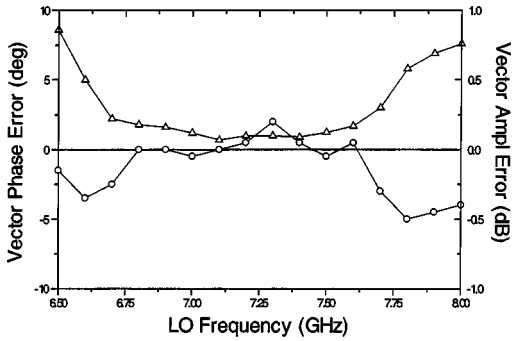


Fig. 19. Measured vector phase (- △ -) and amplitude (- ∘ -) error as a function of LO frequency.

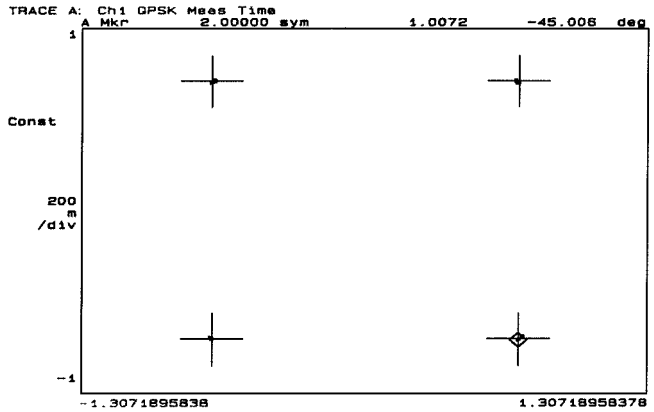


Fig. 20. Measured QPSK constellation: a nearly perfect constellation can be observed.

−34 dB). The measured image rejection is −34 dB, while the carrier suppression (2 × LO) is −43 dB.

The image rejection has also been measured as a function of LO frequency (Fig. 18): in the design band, the image rejection is better than −28 dB, while in the VSAT band, the image rejection is even better than −32 dB. It should be emphasized that this result has been obtained without any on- or off-chip amplitude or phase tuning.

Constellation measurements have been performed, which confirm the previous results. The measured vector amplitude and phase error are given in Fig. 19: the vector phase error remains below 2° and 0.2 dB over the 6.7–7.6-GHz band. The low vector amplitude and phase error result in a nearly perfect constellation, as can be seen in Fig. 20.

The LO return loss of the modulator is better than −13 dB, while the RF return loss is better than −18 dB. The flatness of the output spectrum is somewhat lower than for the BPSK modulator due to the presence of the Lange coupler; however, the conversion loss is still in the range of (−14±0.5) dB over the 6.8–7.5-GHz LO band.

## VI. Conclusion

A direct $Ku$-band linear subharmonically pumped BPSK and I/Q vector modulator has been developed using multilayer thin-film MCM-D technology. All passives are integrated in the low cost MCM-D substrate, while the subharmonic mixing is performed using a beam-lead APDP, mounted onto the MCM using thermocompression. To the authors knowledge, this is the first modulator based on thin-film integrated passive components.

The custom diode model has been verified using nonlinear network analyzer measurements and an excellent agreement has been demonstrated between the measured and simulated powers and phases for more than nine harmonics. It is shown that an optimal reactive termination for the third harmonic of the LO exists such that a very flat mixer conversion loss can be obtained. The input impedances are constant in the same region, which is required to obtain good and constant LO and RF matching. The proposed design method was confirmed by the BPSK measurements showing only a $\pm 0.25$-dB variation on the conversion loss for an LO frequency varying from 6.8 to 7.6 GHz. The measured and simulated conversion loss were in excellent agreement.

The I/Q vector modulator consists of a Wilkinson power divider, a CPW Lange coupler, and two BPSK modulators. The resulting QPSK modulator has a measured image rejection better than $-32$ dB over the VSAT operation band (RF: 14–14.5 GHz).

These results have been obtained without any on- or off-chip amplitude or phase tuning. The circuit also does not require any dc bias.

## References


[1] K. Itoh, M. Shimozawa, K. Kawakami, A. Iida, and O. Ishida, "Even harmonic quadrature modulator with low vector modulation error and low distortion for microwave digital radio," in *IEEE MTT-S Int. Microwave Symp. Dig.*, San Francisco, CA, June 17–21, 1996, pp. 967–970.

[2] P. Boutet, J. Dubouloy, M. Soulard, and J. Pinho, "Fully integrated QPSK linear vector modulator for space applications in $Ku$-band," in *European Microwave Conf.*, Amsterdam, The Netherlands, Oct. 5–9, 1998, pp. 389–392.

[3] W. Philibert and R. Verbiest, "A subharmonically pumped I/Q vector modulator MMIC for $Ka$-band satellite communication," in *IEEE RFIC Symp. Dig.*, Boston, MA, June 11–16, 2000, pp. 183–186.

[4] C. Boulanger, L. Lapierre, and F. Gizard, "New cold FET I-Q linear vector modulator topology," in *Gallium–Arsenide Applicat. Symp.*, Paris, France, Oct. 2–3, 2000, pp. 421–423.

[5] M. Cohn, J. E. Degenford, and B. A. Newman, "Harmonic mixing with an antiparallel diode pair," *IEEE Trans. Microwave Theory Tech.*, vol. MTT-23, pp. 667–673, 1975.

[6] K. Vaesen, P. Pieters, G. Carchon, W. De Raedt, E. Beyne, A. Naem, and R. Kohlmann, "Integrated passives for a DECT VCO," in *Int. High-Density Interconnect Syst. Packag. Conf. Exhib.*, Denver, CO, Apr. 2000, pp. 537–541.

[7] K. Vaesen, S. Donnay, P. Pieters, G. Carchon, W. Diels, P. Wambacq, W. De Raedt, E. Beyne, M. Engels, and I. Bolsens, "Chip-package co-design of a 4.7 GHz VCO," in *Int. High-Density Interconnect Syst. Packag. Conf. Exhib.*, Denver, CO, Apr. 26–28, 2000, pp. 301–306.

[8] G. Carchon, K. Vaesen, S. Brebels, W. De Raedt, B. Nauwelaers, and E. Beyne, "Chip-MCM co-design of a 14 GHz LNA," presented at the Int. High-Density Interconnect Syst. Packag. Conf. Exhib., Santa Clara, CA, Apr. 17–20, 2001.

[9] G. Carchon, P. Pieters, K. Vaesen, S. Brebels, D. Schreurs, S. Vandenberghe, W. De Raedt, B. Nauwelaers, and E. Beyne, "Design-oriented measurement-based scalable models for multilayer MCM-D integrated passives. Implementation in a design library offering automated layout," in *Int. High-Density Interconnect Syst. Packag. Conf. Exhib.*, Denver, CO, Apr. 26–28, 2000, pp. 196–201.

[10] G. Carchon, S. Brebels, K. Vaesen, P. Pieters, D. Schreurs, S. Vandenberghe, W. De Raedt, B. Nauwelaers, and E. Beyne, "Accurate measurement and characterization of MCM-D integrated passives up to 50 GHz," in *Int. High-Density Interconnect Syst. Packag. Conf. Exhib.*, Denver, CO, Apr. 26–28, 2000, pp. 307–312.

[11] G. Carchon, S. Brebels, W. De Raedt, and B. Nauwelaers, "Accurate measurement and characterization up to 50 GHz of CPW-based integrated passives in microwave MCM-D," in *Electron. Comp., Technol. Conf.*, Las Vegas, NV, May 21–24, 2000, pp. 459–464.

[12] G. Carchon, W. De Raedt, and B. Nauwelaers, "Accurate measurement and characterization of reciprocal 3-ports, application to CPW T-junctions in thin-film multi-layer MCM-D," in *Asia–Pacific Microwave Conf.*, Sydney, Australia, Dec. 3–6, 2000, pp. 453–456.

[13] S. A. Maas, *Microwave Mixers*, 2nd ed. Norwood, MA: Artech House, 1993.

[14] D. Schreurs, "Measurement based modeling of heterojunction field-effect devices for nonlinear microwave circuit design," Ph.D. dissertation, ESAT-TELEMIC, K. U. Leuven, Leuven, Belgium, 1997.

[15] J. Verspecht, P. Debie, A. Barel, and L. Martens, "Accurate on wafer measurement of phase and amplitude of the spectral components of incident and scattered voltage waves at the signal ports of a nonlinear microwave device," in *IEEE MTT-S Int. Microwave Symp. Dig.*, Orlando, FL, May 16–20, 1995, pp. 1029–1032.

[16] A. Madjar, "A novel general approach for the optimum design of microwave and millimeter wave subharmonic mixers," *IEEE Trans. Microwave Theory Tech.*, vol. 44, pp. 1997–2000, Nov. 1996.

[17] G. Carchon, W. De Raedt, and B. Nauwelaers, "Integrated Wilkinson power dividers in $C$-, $Ku$- and $Ka$-band in multi-layer thin-film MCM-D," in *European Microwave Conf.*, Paris, France, Oct. 2–6, 2000, pp. 171–174.

[18] G. Carchon, W. De Raedt, E. Beyne, and B. Nauwelaers, "Integration of CPW quadrature couplers in multi-layer thin-film MCM-D," *IEEE Trans. Microwave Theory Tech.*, to be published.


**Geert J. Carchon** (S'97) received the M.Sc. degree in electrical engineering and the Ph.D. degree from the Katholieke Universiteit Leuven (K. U. Leuven), Leuven, Belgium in 1996 and 2001, respectively.

From 1997 to 2000, he was a Research Assistant at the Flemish Institute for the Advancement of Scientific Technological Research in Industry (IWT), K. U. Leuven. Since 2001, he has been involved with the High-Density Interconnect and Packaging Group, Interuniversity Microelectronics Centre (IMEC), Leuven, Belgium. His main interests include the measurement, characterization, and modeling of passive devices and the design of RF and microwave circuits in MMIC and multilayer MCM-D.

**Dominique M. M.-P. Schreurs** (S'90–M'97) received the M.Sc. degree in electronic engineering and the Ph.D. degree (with honors) from the Katholieke Universiteit Leuven (K. U. Leuven), Leuven, Belgium, in 1992 and 1997, respectively.

She is currently a Post-Doctoral Fellow of the Fund for Scientific Research-Flanders and a Visiting Assistant Professor at the K. U. Leuven. Her main research interest is the use of vectorial large-signal measurements for the characterization and modeling of nonlinear microwave devices.

**Walter De Raedt** received the M.Sc. degree in electrical engineering from the Katholieke Universiteit Leuven (K. U. Leuven), Leuven, Belgium, in 1981.

He subsequently became a Research Assistant with the Electronics, Systems, Automation, and Technology (ESAT) Laboratory, where he was involved with direct-write E-beam technology. In 1984, he was with the Interuniversity Microelectronics Centre (IMEC), Leuven, Belgium, where he was involved with research on MMICs and submicrometer technologies for advanced high electron-mobility transistor (HEMT) devices. Since 1997, he has been with the High Density Interconnect and Packaging Group, IMEC, where he is involved with integrated passives and interconnections for RF front-end systems.

**Paul Van Loock** received the M.Sc. degree in electrical engineering from the Katholieke Universiteit Leuven (K. U. Leuven), Leuven, Belgium, in 1982.

In 1982, he joined Alcatel Bell, Antwerp, Belgium, where he was involved in design and development of microwave equipment and systems, mainly in frequency generation for satellite on-board applications. He was responsible for several European Space Agency (ESA) projects such as Artemis $S/Ka$-band payload equipment, advanced synthesized LOs, and on-board modulation/frequency generation. Since 1992, he has been the Head of the RF Development Team, Alcatel Bell Space, Hoboken, Belgium. He is currently involved in the field of advanced VSAT terminals and $Ka$-band converters for TT&C applications.

**Bart K. J. C. Nauwelaers** (S'80–M'86–SM'99) received the M.Sc. and Ph.D. degrees in electrical engineering from the Katholieke Universiteit Leuven (K. U. Leuven), Leuven, Belgium in 1981 and 1988, respectively, and the Mastère degree from the Ecole Nationale Supérieure des Télécommunications (ENST), Paris, France.

Since 1981, he has been with the Electronics, Systems, Automation, and Technology (ESAT) Laboratory, K. U. Leuven, where he has been involved in research on microwave antennas, microwave integrated circuits and MMICs, and wireless communications. He also teaches courses on microwave engineering, analog and digital communications, wireless communications, and design in electronics and telecommunications.